Biogeosciences

Open Access

EGU

Investigating the effect of El Niño on nitrous oxide distribution in the eastern tropical South Pacific

Qixing Ji[1], **Mark A. Altabet**[2], **Hermann W. Bange**[1], **Michelle I. Graco**[3], **Xiao Ma**[1], **Damian L. Arévalo-Martínez**[1], and **Damian S. Grundle**[1,4]

[1]GEOMAR Helmholtz Centre of Ocean Research Kiel, Kiel, 24105, Germany
[2]School for Marine Science & Technology, University of Massachusetts Dartmouth, New Bedford, Massachusetts, USA
[3]Dirección General de Investigaciones Oceanográficas y cambio Climático, Instituto del Mar del Perú (IMARPE),
P.O. Box 22, Callao, Perú
[4]Bermuda Institute of Ocean Sciences, St. George's, GE01, Bermuda

Correspondence: Qixing Ji (qji@geomar.de)

Abstract. The open ocean is a major source of nitrous oxide (N_2O), an atmospheric trace gas attributable to global warming and ozone depletion. Intense sea-to-air N_2O fluxes occur in major oceanic upwelling regions such as the eastern tropical South Pacific (ETSP). The ETSP is influenced by the El Niño–Southern Oscillation that leads to inter-annual variations in physical, chemical, and biological properties in the water column. In October 2015, a strong El Niño event was developing in the ETSP; we conduct field observations to investigate (1) the N_2O production pathways and associated biogeochemical properties and (2) the effects of El Niño on water column N_2O distributions and fluxes using data from previous non-El Niño years. Analysis of N_2O natural abundance isotopomers suggested that nitrification and partial denitrification (nitrate and nitrite reduction to N_2O) were occurring in the near-surface waters; indicating that both pathways contributed to N_2O effluxes. Higher-than-normal sea surface temperatures were associated with a deepening of the oxycline and the oxygen minimum layer. Within the shelf region, surface N_2O supersaturation was nearly an order of magnitude lower than that of non-El Niño years. Therefore, a significant reduction of N_2O efflux (75 %–95 %) in the ETSP occurred during the 2015 El Niño. At both offshore and coastal stations, the N_2O concentration profiles during El Niño showed moderate N_2O concentration gradients, and the peak N_2O concentrations occurred at deeper depths during El Niño years; this was likely the result of suppressed upwelling retaining N_2O in subsurface waters. At multiple stations, water-column inventories of N_2O within the top 1000 m were up to 160 % higher than those measured in non-El Niño years, indicating that subsurface N_2O during El Niño could be a reservoir for intense N_2O effluxes when normal upwelling is resumed after El Niño.

1 Introduction

The El Niño–Southern Oscillation (ENSO) is a naturally occurring decadal climate cycle that affects the oceanic and atmospheric conditions across the equatorial Pacific (Philander, 1983). A pronounced effect of ENSO in the ocean is the redistribution of heat flux across the tropical and subtropical Pacific. Generally, the ENSO cycle can be divided into three phases, El Niño, La Niña, and neutral. During El Niño/La Niña years, higher/lower sea surface temperature and deepening/shoaling of the thermocline depth occur in the eastern tropical South Pacific (ETSP) (Barber and Chavez, 1983). During El Niño years, upwelling is suppressed in the ETSP, and thus reduces upward nutrient fluxes to the surface waters causing decreased primary production (Chavez et al., 2003; Ñiquen and Bouchon, 2004; Graco et al., 2017).

The ETSP is an oceanic region with intense sea-to-air flux of nitrous oxide (N_2O), a strong greenhouse gas and a potent ozone-depleting agent in the 21st century (Ravishankara et al., 2009). Diverse microbial processes involved in the production and consumption of N_2O occur in the ETSP, a major

oceanic oxygen minimum zone (OMZ) having a wide range of O_2 concentrations spanning the sub-nanomolar level at intermediate depths (Revsbech et al., 2009) to atmospheric saturation at the surface. In the presence of oxygen, N_2O is a by-product during the first step of nitrification, i.e., ammonium (NH_4^+) oxidation to nitrite (NO_2^-) (Anderson, 1964). Under suboxic and anoxic conditions, N_2O is produced via partial denitrification, i.e., NO_2^- reduction and nitrate (NO_3^-) reduction (Codispoti and Christensen, 1985). Partial denitrification can be mediated by denitrifying bacteria using NO_2^- and NO_3^- as substrates, as well as nitrifying bacteria using only NO_2^-, a process termed nitrifier–denitrification (Frame and Casciotti, 2010; Trimmer et al., 2016). The dominant biological sink of N_2O in the ocean is the last step of denitrification where N_2O is reduced to N_2 under anoxic conditions (Codispoti and Christensen, 1985). Recent investigations suggest that N_2O uptake by diazotrophs is another possible N_2O sink occurring at the surface waters (Farías et al., 2013; Cornejo et al., 2015). Its environmental significance awaits further exploration.

Research on the impact of ENSO on N_2O dynamics was initiated by the observation of significant reduction in oceanic N_2O effluxes during El Niño events (Cline et al., 1987; Butler et al., 1989). Recent model simulations demonstrated that ENSO events could induce lower denitrification rates, higher nitrification rates, and lower N_2O fluxes (Mogollón and Calil, 2017; Yang et al., 2017), which could be related to changes in O_2 and organic matter availabilities that are critical environmental factors regulating N_2O production (Elkins et al., 1978; Farías et al., 2009; Arévalo-Martínez et al., 2015; Kock et al., 2016). Here we report water column hydrography, nitrogen biogeochemistry, and N_2O distribution during October 2015 when a strong El Niño event (recurrence interval > 10 years) was developing (Stramma et al., 2016; Santoso et al., 2017). The natural abundance isotopomers of N_2O, i.e., the intramolecular configuration of stable isotopes (^{15}N vs. ^{14}N and ^{18}O vs. ^{16}O), were used to determine the pathways of N_2O production and consumption by a simple mass balance model outlined previously (Yamagishi et al., 2007; Grundle et al., 2017). Finally, the effects of a strong El Niño event on the surface and water column N_2O distributions were investigated by incorporating archived ETSP datasets that demonstrated contrasting hydrography and biogeochemistry between El Niño and non-El Niño years.

2 Materials and methods

2.1 Field sampling and laboratory measurements

The progress and the strength of El Niño was quantified by the Ocean Niño Index (ONI, Fig. 1), defined as the running 3-month average sea surface temperature anomaly for the Niño 3.4 region in the east-central tropical Pacific (5° S–5° N,
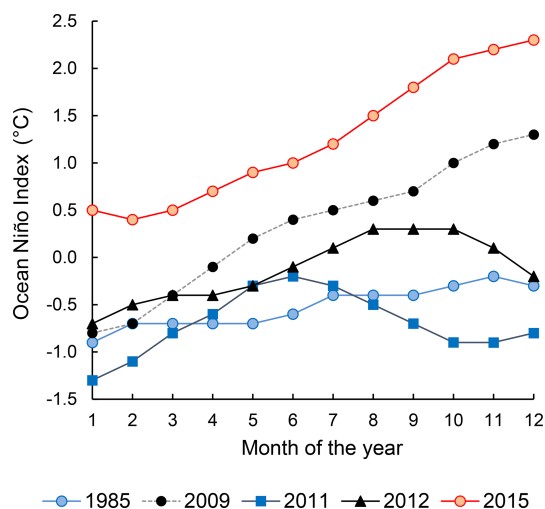

Figure 1. Ocean Niño Index of the years 1985 (weak La Niña), 2009 (neutral), 2011 (weak La Niña), 2012 (neutral), and 2015 (strong El Niño). Data were downloaded from http://origin.cpc.ncep.noaa.gov/products/analysis_monitoring/ensostuff/ONI_v5.php (last access: 15 October 2018).

120–170° W). The 2015–2016 El Niño was a "strong El Niño event" indicated by ONI ≥ 0.5 °C from November 2014 to May 2016. This study was conducted on the ASTRA-OMZ SO243 cruise on board the R/V *Sonne* between 5 and 22 October 2015 from Guayaquil, Ecuador, to Antofagasta, Chile (Fig. 2a). In October 2015, the El Niño was still developing with ONI = 2.1 °C, comparable to other strong El Niño events in 1972–1973, 1982–1983, and 1997–1998 (Stramma et al., 2016).

The sampling stations are categorized into offshore (Fig. 2a in red polygon) and coastal (Fig. 2a white polygon) according to their respective water depth: the coastal stations are shallower than 250 m whereas the offshore stations are > 3000 m in depth. Water samples were taken from a 24 × 10 L bottle CTD rosette system. At every station, CTD Niskin bottles collected water samples at 10–20 depths spanning the observed oxygen concentration range. The CTD system was equipped with two independent sets of sensors for temperature, conductivity (salinity), and oxygen measurements. Calibrations for temperature, salinity, and oxygen measurements were reported previously, with standard deviations of 0.002 °C, 0.0011 PSU, and 0.8 µmol L^{-1} [O_2], respectively (Stramma et al., 2016). The detection limit of dissolved oxygen was ~ 3 µmol L^{-1}; the oxygen-deficient zone (ODZ) was operationally defined as water parcels with [O_2] < 5 µmol L^{-1}, and the upper and lower oxycline boundary layer was defined as [O_2] = 20 µmol L^{-1} isoline occurring above and below the ODZ, respectively. Saturation level of O_2 was calculated with in situ temperature and salinity according to Garcia and Gordon (1992). Dissolved NO_3^- and NO_2^- concentrations were measured at sea with an auto-analyzer (QuAAtro, Seal Analytical, Germany). Chemical

analyses of NO_3^- and NO_2^- had detection limits of 0.1 and $0.02\,\mu mol\,L^{-1}$, respectively. For N_2O concentration measurements, triplicate samples were collected in 20 mL brown glass vials and were crimp-sealed with butyl stoppers and aluminum caps. Immediately following this, a 10 mL helium headspace was created and 50 μL of saturated mercuric chloride ($HgCl_2$) solution was added. After an equilibration period of at least 2 h, the headspace sample (10 mL) was measured by a gas chromatograph equipped with an electron capture detector (GC/ECD) that was calibrated on a daily basis using dilutions of two standard gas mixtures. The detailed GC/ECD setup and calculation of N_2O concentration were reported previously (Walter et al., 2006; Kock et al., 2016). For the N_2O concentration data of the 2015 cruise, the standard deviation of triplicate sampling was 1 %–8 %, generally $< 2.5\,nmol\,L^{-1}$.

Water column N_2O saturation was quantified by the N_2O excess (ΔN_2O), defined as the concentration difference between measured and equilibrium values:

$$\Delta N_2O = [N_2O]_{measured} - [N_2O]_{equilibrium}. \tag{1}$$

The N_2O equilibrium concentration was calculated according to Weiss and Price (1980) with in situ temperature, salinity, and the atmospheric N_2O dry mole fraction in the year of 2015, 328 ppb at 1 atmospheric pressure (Blasing, 2016). The N_2O efflux from the ocean to the atmosphere was calculated as the product of N_2O excess and gas transfer coefficient (k_w, $cm\,h^{-1}$) that was derived according to the empirical relationship proposed by Wanninkhof (2014):

$$k_w = 0.251 \times U_{10}^2 \times (Sc/660)^{-0.5}, \tag{2}$$

where U_{10} denotes wind speed ($m\,s^{-1}$) at 10 m above sea surface, and Sc denotes the Schmidt number for N_2O under in situ temperature (Wanninkhof, 2014).

Samples for natural abundance N_2O isotopes and isotopomers were collected in 160 mL glass serum bottles with butyl stoppers and aluminum seals and preserved with 100 μL of saturated $HgCl_2$. Isotopomeric measurements of N_2O were carried out at the University of Massachusetts Dartmouth following procedures previously reported (Grundle et al., 2017). In brief, dissolved N_2O was extracted by an automated purge-and-trap system and concentrated with liquid nitrogen. Interfering molecules such as H_2O and CO_2 were isolated from N_2O to increase measurement precision. A multi-collector isotope ratio mass spectrometer detected intact N_2O molecule mass ratios of 45/44 and 46/44 and a NO^+ fragment mass ratios 31/30. Relative abundance of N_2O isotopomers was expressed using the delta notation (δX), defined as the relative difference between isotopic ratio (R) of sample and reference material:

$$\delta X = \left(\frac{R_{sample}}{R_{reference}} - 1 \right) \times 1000, \tag{3}$$

where X denotes $^{15}N_\alpha$, $^{15}N_\beta$, and ^{18}O, and R denotes the $^{15}N/^{14}N$ at the central (α) and terminal (β) nitrogen posi-

tions and $^{18}O/^{16}O$ at oxygen position of the N_2O molecule. The value of δX is expressed as per mill (‰) deviation relative to a set of reference materials: atmospheric N_2 for $\delta^{15}N_{bulk}$, $\delta^{15}N_\alpha$, and $\delta^{15}N_\beta$ (Mohn et al., 2014), and Vienna standard mean ocean water (VSMOW) for $\delta^{18}O$. Therefore, mass ratios of 45/44, 46/44, and 31/30 determined $\delta^{15}N_{bulk}$ (conventionally $\delta^{15}N$), $\delta^{18}O$, and $\delta^{15}N_\alpha$, respectively. The $\delta^{15}N_\beta$, the relative abundance of N_2O molecule with ^{15}N substitution at the terminal (β) position, was calculated by $\delta^{15}N_\beta = 2 \times \delta^{15}N_{bulk} - \delta^{15}N_\alpha$. Site preference (SP) is defined as follows:

$$SP = \delta^{15}N_\alpha - \delta^{15}N_\beta. \tag{4}$$

Calibration of $\delta^{15}N_\alpha - N_2O$, $\delta^{15}N_\beta - N_2O$, and $\delta^{18}O - N_2O$ was accomplished using four certified standard gases (supplied by Joachim Mohn; see Table S2 in the Supplement) encompassing the values reported here. The analytical precision of isotope measurements was ± 0.07, 0.17, 0.36, and 0.18 ‰ for $\delta^{15}N_{bulk}$-N_2O, $\delta^{15}N_\alpha - N_2O$, $\delta^{15}N_\beta - N_2O$, and $\delta_{18}O - N_2O$, respectively.

2.2 Additional datasets

The twice-weekly, 50 km resolution of sea surface temperature anomaly data from NOAA's Satellite Coral Bleaching Monitoring Datasets (https://coralreefwatch.noaa.gov/satellite/methodology/methodology.php, last access: 15 October 2018) were used to quantify the sea surface temperature difference of the ETSP during October 2015 relative to 1985–1993. For N_2O flux calculations, instantaneous wind speed data at each of our sampling locations were acquired from shipboard metrological measurements. Seawater N_2O and oxygen concentrations from previous sampling campaigns in the ETSP were extracted from the MEMENTO database (Kock and Bange, 2015). Specifically, data from the following cruises were used for comparison between El Niño and non-El Niño years: NITROP-85 (February 1985), M77/3 (January 2009), Callao Time Series Transect (October 2011), M90 (November 2012), M91 (December 2012), and AT26-26 (January 2015). The ONI of these years (1985, 2009, 2011, 2012, Fig. 1) indicated that 1985 and 2011 are considered weak La Niña years, whereas 2009 and 2012 are considered neutral years. The MEMENTO database has not archived any N_2O datasets in the ETSP region during previous El Niño events, and therefore we were not able to compare N_2O dynamics between two El Niño time periods. To facilitate the comparison, the 2015 and archived N_2O depth profiles were compared at three offshore and three coastal locations, each within a grid space of $0.75° \times 0.75°$ (see Table S1 for station coordinates). Standard deviations of repeated N_2O concentration measurements (analytical precision) for archived N_2O concentration datasets were retrieved from respective references (see Table S1). These analytical precisions are $< 5\%$ of N_2O concentration values.
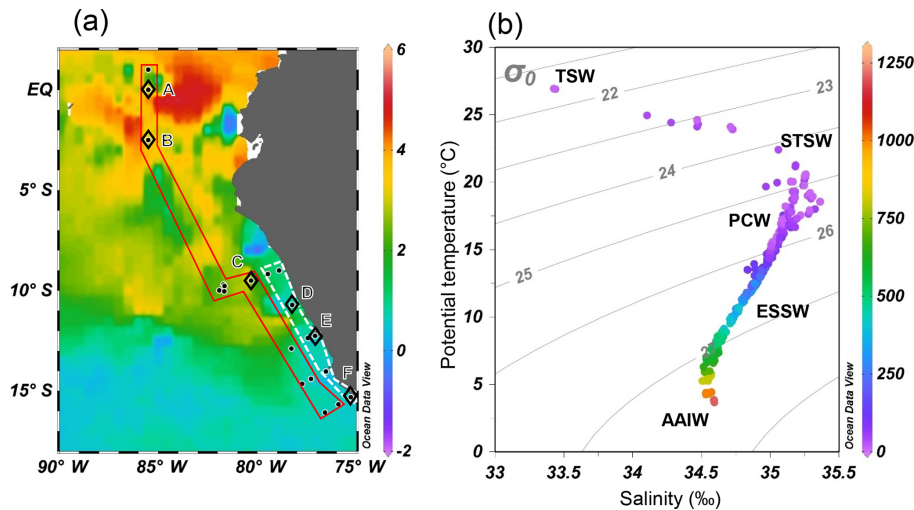
Figure 2. (a) Monthly mean sea surface temperature anomaly (°C) of October 2015 from NOAA's Satellite Coral Bleaching Monitoring Datasets. Sampling stations (filled circles) are categorized as "offshore" (in red polygon) and "coastal" sections (in white polygon). Comparative analyses of water column N_2O (see Sect. 4.3) were performed at stations A–E (open diamonds). **(b)** Potential temperature–salinity diagram, with corresponding depths (meters, color bar on right) and potential density (σ_θ, kg m^{-3}) of all sampling stations. Five water masses are shown: tropical surface water (TSW), subtropical surface water (STSW), Peru coastal water (PCW), equatorial subsurface water (ESSW), and Antarctic intermediate water (AAIW).

3 Results

3.1 Hydrography, distribution of oxygen, and inorganic nitrogen

The 2015–2016 El Niño event impacted the ETSP with a relatively high sea surface temperature anomaly, especially at the equatorial region (2° S–2° N and 80–90° W) where the highest anomaly between 3 and 5 °C was observed at offshore waters (Fig. 2a). The El Niño-induced warming effect decreased southwards. Between 5 and 12° S, the temperature anomaly was 2–3 °C. South of 12° S the anomaly was generally < 1 °C. The shelf areas between 7 and 14° S had a progressively lower temperature anomaly southwards: > 1.5 and < 1 °C north and south of 12° S.

Five water masses, based on their thermohaline indices (Strub et al., 1998; Silva et al., 2009), were identified (Fig. 2b). The northward-flowing Antarctic Intermediate water (AAIW, $T = 3$–5 °C, $S \approx 34.5$) was found at depths below 1000 m. The equatorial subsurface water (ESSW, $T = 8$–12 °C, $S = 34.7$–34.9) was near the Peruvian coast at depths between 300 and 400 m. Above the continental slope (water depth < 250 m), the colder Peru coastal water (PCW, $T < 19$ °C, $S \approx 35$) occupied 30–250 m, whereas the warmer subtropical surface water (STSW, $T > 18.5$ °C, $S > 34.9$) was found at depth < 30 m. The surface water north of the Equator consisted of the tropical surface water (TSW), which had high temperature and low salinity ($T > 25$ °C, $S < 33.5$) due to excess precipitation. The October 2015 water column below 250 m had similar thermohaline properties compared to those of October–December 2012 (non-El Niño) that had

been shown in an earlier study (Kock et al., 2016), except that October 2015 had 2–4 °C warmer surface water.

Along the offshore section, the upper oxycline boundary ([O_2] = 20 μmol L^{-1} isoline) was at 250–300 m along the Equator at 85.5° W, and the ODZ ([O_2] < 5 μmol L^{-1}) appeared near 10° S (Fig. 3a). The southward shoaling of the oxycline, thickening of the ODZ, and shoaling of the [NO_3^-] = 20 μmol L^{-1} isoline were observed south of 10° S (Fig. 3a and b), where the thickness of the ODZ was ∼ 300 m. The top of the ODZ reached ∼ 125 m between 13 and 16° S. Significant accumulation of NO_2^- (> 1 μmol L^{-1}) occurred south of 10° S between 30 and 400 m within the ODZ (Fig. 3c), corresponding to lower NO_3^- concentrations (Fig. 3b). The highest NO_2^- concentration (9.4 μmol L^{-1}) was recorded at 200 m at 15.7° S.

Along the coastal section, the surface (upper 10 m) O_2 concentrations were below saturation at all sampling stations (50 %–97 % saturation). Surface O_2 concentrations were 165–217 μmol L^{-1} north of 10° S and gradually decreased to 135–190 μmol L^{-1} between 10 and 12.5° S and to 120 μmol L^{-1} south of 14° S (Fig. 3d). The shoaling of the [O_2] = 20 μmol L^{-1} isoline was observed south of 9° S. The top of the ODZ was found at 200, 150, and 80 m at 11, 12, and 14° S, respectively. The surface NO_3^- concentrations were 11–23 μmol L^{-1} between 9 and 16° S, and the [NO_3^-] = 20 μmol L^{-1} isoline was at 0–20 m (Fig. 3e). Water column NO_2^- concentrations at coastal stations were generally below 1 μmol L^{-1}, with the exception of the station at 14.0° S where NO_2^- concentrations reached 1.2 μmol L^{-1} below 200 m (Fig. 3f).

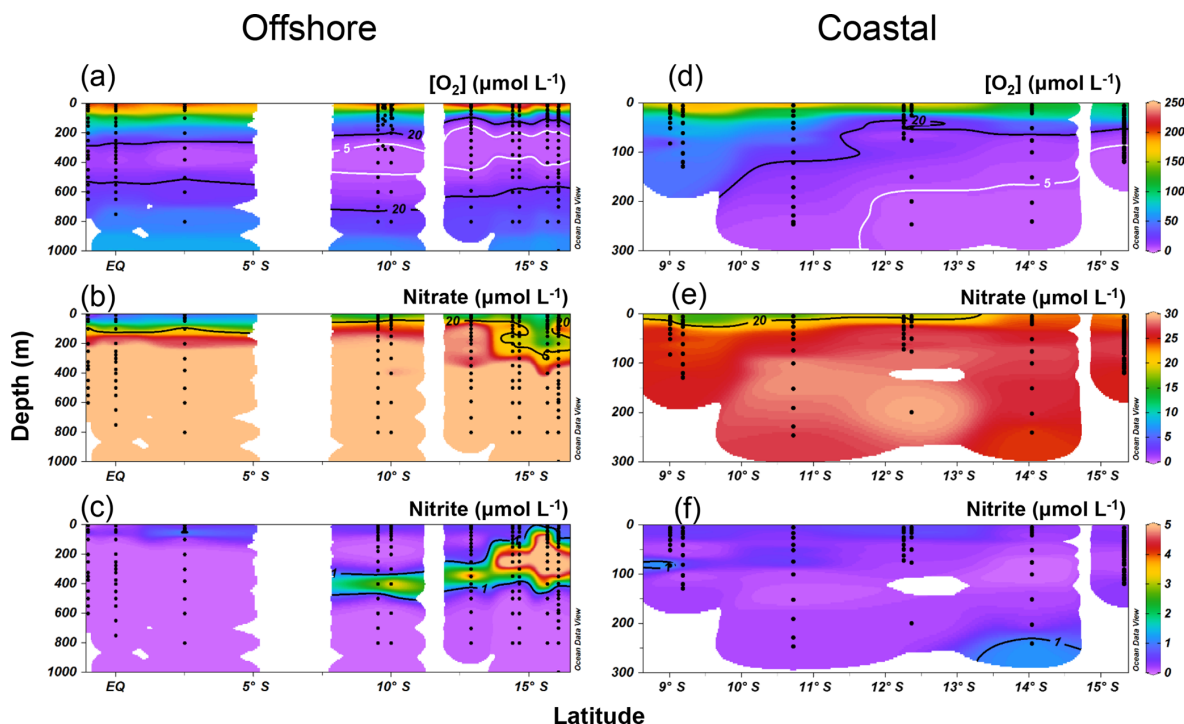**Figure 3.** Water column oxygen (**a, d**), nitrate (**b, e**), and nitrite concentrations (**c, f**) along the offshore (**a, b, c**) and coastal sections (**d, e, f**) during October 2015.

3.2 Water column N$_2$O concentrations and isotopes

Along the offshore section, the water column N$_2$O distributions showed a southward increase in surface concentrations and southward decrease in subsurface concentration maxima (Fig. 4a). The equatorial region (1° N to 2.5° S, 85.5° W) had subsurface N$_2$O concentrations up to 93 nmol L^{-1} at thermocline depths (200–550 m); water column δ^{15}N, SP, and δ^{18}O generally increased with depth (Fig. 4b, c and d); at the subsurface N$_2$O concentration maximum, δ^{15}N, SP, and δ^{18}O were ~ 6‰, 13‰–17‰, and 45‰–50‰, respectively. Two N$_2$O concentration maxima were observed at stations south of 10° S where the ODZ was formed. Near 10° S, two N$_2$O concentration maxima (70 ± 6 nmol L^{-1}) occurred between 200 and 600 m; and a local concentration minimum (~ 30 nmol L^{-1}) occurred within the ODZ at 400 m, associated with high δ^{15}N (8‰–10‰), SP (20‰–30‰), and δ^{18}O (60‰–70‰). Near 13° S, a shallow N$_2$O concentration maximum (~ 80 nmol L^{-1}) occurred at ~ 100 m, and a local N$_2$O concentration minimum (18 nmol L^{-1}) occurred at 350 m. Between 14 and 16° S, the lowest (< 10 nmol L^{-1}) N$_2$O concentrations were observed at 200–400 m within the ODZ, where the highest values of δ^{15}N (> 10‰), SP (30‰–40‰), and δ^{18}O (> 60‰) were observed.

Along the coastal section, a southward increase in surface N$_2$O concentration (20 nmol L^{-1} north of 11° S and > 40 nmol L^{-1} south of 13° S) was observed, coinciding with southward shoaling of the ODZ (Fig. 4e). Subsurface maximum N$_2$O concentrations were observed below 200 m near 10.7° S and at 80–90 m south of 12° S, where ODZ was formed. The δ^{15}N values in coastal waters were between 2.5 and 5‰, with lower values at stations south of 14°S (Fig. 4f). SP was lower (−10‰ to 0‰) at the surface (< 10 m) near 9° S and at 50–150 m near 11°S; higher SP (10‰–20‰) was observed south of 14°S (Fig. 4g). The δ^{18}O values were 45‰–60‰; higher δ^{18}O (> 55‰) values were observed within the ODZ below 200 m at 14°S and below 100 m at 15.3° S (Fig. 4h).

3.3 Excess N$_2$O and N$_2$O flux to the atmosphere

Both the offshore and coastal stations showed N$_2$O supersaturation in the top 10 m of surface water, and coastal stations had higher ΔN$_2$O concentrations (15–50 nmol L^{-1}) than those of offshore stations (4–8 nmol L^{-1}). Subsurface ΔN$_2$O along the offshore section had higher concentrations at the equatorial regions (70–80 nmol L^{-1}) than ΔN$_2$O concentrations at stations located south of 10° S (40–60 nmol L^{-1}, Fig. 5a). Near 15° S, subsurface N$_2$O undersaturation was observed; ΔN$_2$O concentrations were −4 to 0 nmol L^{-1} at thermocline depths (200–400 m) within the ODZ ([O$_2$] < 5 µmol L^{-1}). Along the coastal section, a southward increase in surface and subsurface (50–200 m) ΔN$_2$O was observed (Fig. 5b). Subsurface maximum ΔN$_2$O concentrations were > 60 nmol L^{-1}, and occurred at the periphery of ODZ (~ 200 m near 10° S and < 100 m south of 12° S). Undersat-
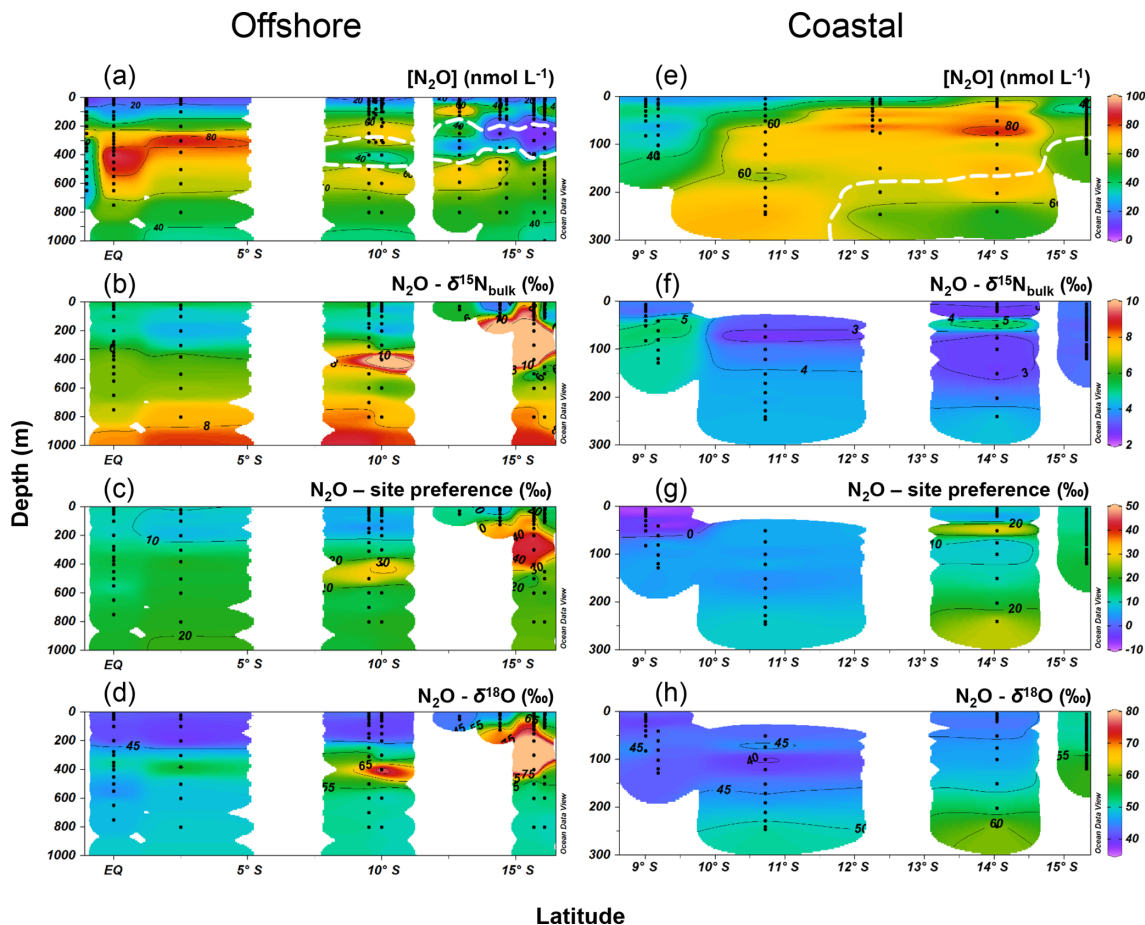
Figure 4. Water column N_2O concentrations **(a, e)**, $\delta^{15}N_{bulk}$ **(b, f)**, site preference **(c, g)**, and $\delta^{18}O$ **(d, h)** along the offshore **(a, b, c, d)** and coastal sections **(e, f, g, h)** during October 2015. White contour lines in **(a)** and **(e)** denote the boundary of the oxygen-deficient zone ($[O_2] = 5 \, \mu mol \, L^{-1}$ isoline).

uration of N_2O ($\Delta N_2O < 0$) did not occur in any coastal stations. The N_2O fluxes from the coastal stations were 23–$108 \, \mu mol \, m^{-2} \, d^{-1}$, nearly 2-fold the offshore fluxes (7–$50 \, \mu mol \, m^{-2} \, d^{-1}$, Fig. 5c). The highest flux occurred at a coastal station at $14.4°$ S, $77.3°$ W, coinciding with the highest surface ΔN_2O ($50 \, nmol \, L^{-1}$).

4   Discussion

The ETSP is one of the world's major oceanic OMZs having active N_2O production and intense efflux to the atmosphere (Arévalo-Martínez et al., 2015; Kock et al., 2016). The gradient spanning from fully oxygenated conditions to anoxia creates suitable conditions for N_2O production and consumption, which causes the coexistence of water column N_2O supersaturation and undersaturation (Codispoti and Christensen, 1985). To identify the N_2O cycling pathways, we input N_2O isotopic and isotopomeric measurements into a simple mass balance model (Sect. 4.1). Quantitative relationships linking O_2, NO_3^-, and N_2O were examined to char-

acterize the effect of oxygenation on N_2O production from NH_4^+ oxidation (Sect. 4.2). Previously measured N_2O concentrations from the ETSP were extracted from the MEMENTO database (Kock and Bange, 2015) and were compared to data from this study to investigate the contrasting water column N_2O distribution and effluxes between El Niño and non-El Niño years (Sect. 4.3), which would better constrain the natural variability of N_2O cycling in the ETSP.

4.1 N_2O cycling pathways inferred from natural abundance isotopic and isotopomeric signatures

The analyses of natural abundance isotopomers quantify the substitutions of nitrogen and oxygen isotopes occurring on the linear asymmetric N_2O molecule (Yoshida and Toyoda, 2000), and can be used to identify potential production and consumption pathways (Yamagishi et al., 2007; Grundle et al., 2017). The production of N_2O in an isolated water body follows mass conservation of the respective isotopes and isotopomers. The mass balance model proposed by Fujii et al. (2013) quantified the isotopic signature of N_2O produced
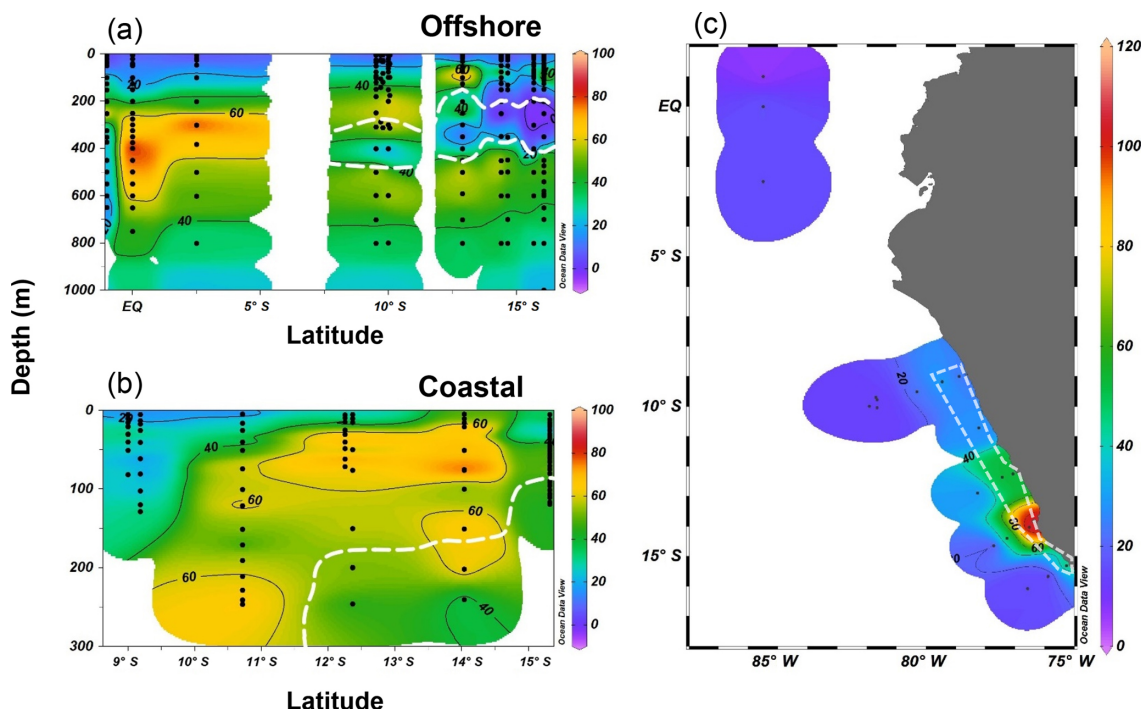
Figure 5. N_2O excess (ΔN_2O, $nmol\,L^{-1}$) at the offshore section **(a)** and the coastal section **(b)** during October 2015; the white dashed line indicates the boundary of the oxygen-deficient zone ($[O_2] = 5\,\mu mol\,L^{-1}$ isoline). **(c)** Surface N_2O efflux ($\mu mol\,m^{-2}\,d^{-1}$) from offshore and coastal stations (enclosed in white polygon) during October 2015.

within the water mass ($\delta_{produced}$) by the linear regression of the inverse N_2O concentration ($1/[N_2O]_{measured}$) and the observed isotope values ($\delta_{observed}$):

$$\delta_{observed} = \frac{[N_2O]_{initial}}{[N_2O]_{measured}} \times \left(\delta_{initial} - \delta_{produced}\right) + \delta_{produced}, \tag{5}$$

where $[N_2O]_{initial}$ and $\delta_{initial}$ refer to source water N_2O concentration and isotopic signature, respectively. It has been shown that SP is only determined by N_2O cycling pathways and that SP is independent of nitrogen isotopic values of the substrates for N_2O cycling. Both culture and field studies demonstrated that N_2O production via NH_4^+ oxidation and partial denitrification (including both nitrifier- and denitrifier-mediated denitrification) are associated with typical SP values of $30 \pm 5\,‰$ and $0 \pm 5\,‰$, respectively (Toyoda et al., 2011). Recent results from culture (Winther et al., 2018) and river water (Mothet et al., 2013) showed that N_2O production via denitrification had SP values as low as $-10\,‰$. Thus, by determining $SP_{produced}$, N_2O cycling processes can be qualitatively characterized. We further identified four water bodies (coastal and offshore stations combined) from shallow to deeper depths with distinctive features such as O_2, NO_2^- concentrations, and depths (Table 1) to discuss N_2O cycling pathways as follows.

1. Upper oxycline and surface (Fig. S1a in the Supplement): $[O_2] > 20\,\mu mol\,L^{-1}$, $[NO_2^-] < 1\,\mu mol\,L^{-1}$, and

depth $< 200\,m$. N_2O production from this water body could actively contribute to atmospheric efflux. The samples had variable SP values ($-9\,‰$ to $34\,‰$); some coastal samples had low SP values ($-5\,‰$ to $-9\,‰$, Fig. 4g), which as outlined above is characteristic of strong denitrifying N_2O production. The low $SP_{produced}$ (6.4 ± 1.9) indicates that both nitrification and denitrification were sources of N_2O to the upper oxycline, with the majority appearing to come from denitrification. Given that the O_2 concentrations were too high for denitrification to proceed locally in the upper oxycline and the surface (Codispoti and Christensen, 1985), the SP signature of N_2O in this water body was a mixture of local nitrification and denitrification signal from the peak N_2O concentration depths (see below) as a result of active upwelling and upward diffusion in the ETSP (Haskell et al., 2015). Thus, denitrification and nitrification both contribute to N_2O effluxes in the ETSP OMZ, consistent with a previous study which focused on the coastal regions between ~ 12 and $14°\,S$ (Bourbonnais et al., 2017).

2. N_2O peak (Fig. S1b): $[O_2] = 5\text{--}20\,\mu mol\,L^{-1}$, $[NO_2^-] < 1\,\mu mol\,L^{-1}$, and depth $= 45\text{--}500\,m$. The samples were from N_2O concentration maxima near the upper boundary of the ODZ. The $SP_{produced}$ is relatively low ($8.3 \pm 3.0\,‰$) at this suboxic water body ($[O_2] < 20\,\mu mol\,L^{-1}$), which allowed N_2O production from

denitrification while inhibiting N_2O consumption (Bonin et al., 1989; Farías et al., 2009). The $SP_{produced}$ leads us to conclude that water column N_2O maximum was mainly attributed to partial denitrification (i.e., NO_2^- and NO_3^- reduction). This is consistent with previous ^{15}N tracer incubation experiments demonstrating that N_2O concentration maximum above the ODZ was likely the result of high rates of N_2O production from NO_2^- and NO_3^- reduction that are 10–100 times higher than the rate of NH_4^+ oxidation to N_2O (Ji et al., 2015).

3. Oxygen-deficient zone (Fig. S1c): $[O_2] < 5\,\mu mol\,L^{-1}$ and $[NO_2^-] > 1\,\mu mol\,L^{-1}$, and depth $= 70$–$400\,m$. The ODZ has prominent features such as the accumulation of NO_2^- (Codispoti and Christensen, 1985), and undersaturation of N_2O as a result of dynamic balance between the concomitant N_2O production (Ji et al., 2015) and consumption by denitrification (Babbin et al., 2015). The isotopic signature of "produced N_2O" had distinctively high $\delta^{15}N_{bulk}$ (8.5 ‰) and $\delta^{18}O$ (71 ‰, Table 1 and Fig. S2), and this is indicative of pronounced N_2O reduction to N_2, which results in an isotope enrichment of the remaining N_2O pool in the process of N–O bond breakage (Toyoda et al., 2017). The SP signature was also high (39.9 ‰). While NH_4^+ oxidation can produce N_2O with similar SP values, we rule this out given the observed low O_2 concentrations (Peng et al., 2016). Instead, similar to the high $\delta^{15}N_{bulk}$ and $\delta^{18}O$ values which were observed, we suggest that the high SP values which were recorded in the ODZ, where N_2O undersaturation occurred, were also a result of N_2O consumption, as reduction of N_2O can also result in high SP values (Popp et al., 2002; Well et al., 2005; Mothet et al., 2013). Based on the observed $\delta^{15}N_{bulk}$, $\delta^{18}O$, and SP values of N_2O, we conclude that N_2O consumption was the predominant N_2O cycling pathway in the water body with $[O_2] < 5\,\mu mol\,L^{-1}$ and $[NO_2^-] > 1\,\mu mol\,L^{-1}$ in the ETSP.

4. Intermediate waters (Fig. S1d): samples from depths 500–1000 m with $[O_2] = 5$–$70\,\mu mol\,L^{-1}$ and $[NO_2^-] < 1\,\mu mol\,L^{-1}$. Generally, the N_2O concentration peak below the ODZ at the offshore waters can be found in this water body (Fig. 4a). From the linear regression, the $SP_{produced}$ is 15.6 ± 4.1 ‰, indicating that both nitrification and denitrification produced N_2O under the oxic and suboxic conditions ($[O_2] = 5$–$70\,\mu mol\,L^{-1}$). Downward mixing and diffusion from the ODZ is unlikely because the ETSP is a major upwelling region and ODZ samples had high SP values (see next paragraph). We conclude that localized N_2O production from nitrification and denitrification is an important pathway in this region of the water column, and probably contributed to N_2O concentration maxima

in intermediate waters, as reported by Carrasco et al. (2017).

There are some limitations of the isotopomer-based analysis of potential N_2O cycling pathways. (1) Constant atmospheric exchange at the surface and mixed layer, and mesoscale eddy activities at intermediate waters (Arévalo-Martínez et al., 2016) could affect the $SP_{produced}$ from localized N_2O cycling. Nevertheless, our conclusion of denitrification being an important pathway remains valid. As a comparison, water bodies were divided by potential density surfaces (i.e., $\sigma_\theta > 27$, 26–27, 25–26, $< 25\,kg\,m^{-3}$) and showing $SP_{produced}$ of 5.0 ‰–11.1 ‰. (2) We are not able to investigate the change in N_2O production rates from nitrification and denitrification that are affected by El Niño-induced lower export production, as demonstrated by Espinoza-Morriberón et al. (2017). With complimentary datasets such as isotopic compositions of NO_3^- and NO_2^-, the rates of N_2O production can be derived by isotopic relationships during N_2O production processes using a three-dimensional biogeochemical model (Bourbonnais et al., 2017).

4.2 The effect of O_2 on N_2O production from NH_4^+ oxidation

The surface and upper oxycline directly contribute to oceanic N_2O effluxes, with NH_4^+ oxidation being the dominant production pathway due to O_2 inhibition of denitrification (see Sect. 4.1). Thus, it is worth investigating N_2O production from NH_4^+ oxidation occurring along the oxygen gradient. During NH_4^+ oxidation to NO_2^-, the effectiveness of N_2O production can be quantified with the N_2O yield, which is defined as the molar nitrogen ratio of N_2O produced and NH_4^+ oxidized. In oxygenated waters, the near absence of NH_4^+ and NO_2^- suggests the amount of NH_4^+ oxidized produces equal amounts of NO_3^- within measurement error. Rees et al. (2011) and Grundle et al. (2012) computed the N_2O yield by deriving the slope of the linear regression of the $\Delta N_2O - NO_3^-$ relationship. The ΔN_2O data from all sampling stations during October 2015 showed that ΔN_2O increases with increasing NO_3^- concentrations and decreasing O_2 concentrations (Fig. 6). The samples from the upper oxycline ($[O_2] > 20\,\mu mol\,L^{-1}$ and depth $> 500\,m$) showed a moderate increase in ΔN_2O (0–20 $nmol\,L^{-1}$) when $[NO_3^-] < 20\,\mu mol\,L^{-1}$. At $[NO_3^-] > 20\,\mu mol\,L^{-1}$, substantial increase in ΔN_2O (20–75 $nmol\,L^{-1}$) was observed. Here, to avoid sampling the ODZ where suboxic conditions stimulate N_2O production from partial denitrification (i.e., water body no. 3 described in Sect. 4.1), only data from the upper oxycline (depth $< 500\,m$) were used to perform linear regression. The slope of the regression at $[NO_3^-] < 20\,\mu mol\,L^{-1}$ (corresponding to $[O_2] > 100\,\mu mol\,L^{-1}$) is 0.85 ± 0.11, indicating that $0.085 \pm 0.011\,nmol$ of N_2O is produced for every micromole of NO_3^- produced (or NH_4^+ oxidized), equating a molar nitrogen yield (mol N_2O-N produced/mol NO_3^-

Table 1. Isotopic signature of N_2O cycling processes estimated by linear regression of isotopomer ratios and inverse N_2O concentrations (see Sect. 4.1 for model description and Fig. S1 for results) in water bodies of upper oxycline and surface, N_2O peak, oxygen-deficient zone, and intermediate waters.

No.	Layer	Definition	Statistical properties	$\delta^{15}N_{bulk}$ (‰)	$\delta^{18}O$ (‰)	SP (‰)
1	Upper oxycline and surface	Depth 0–200 m $[O_2] > 5\,\mu mol\,L^{-1}$ $[NO_2^-] < 1\,\mu mol\,L^{-1}$	Produced N_2O Standard error R^2 ($n = 76$)	2.8 0.3 0.37	45.9 1.2 0	6.4 1.9 0.04
2	N_2O peak	Depth $= 45$–500 m $[O_2] = 5$–$20\,\mu mol\,L^{-1}$ $[NO_2^-] < 1\,\mu mol\,L^{-1}$	Produced N_2O Standard error R^2 ($n = 48$)	5.4 0.9 0.04	41.3 3.0 0.24	8.3 3.0 0.08
3	Oxygen-deficient zone	Depth $= 70$–400 m $[O_2] < 5\,\mu mol\,L^{-1}$ $[NO_2^-] > 1\,\mu mol\,L^{-1}$	Produced N_2O Standard error R^2 ($n = 11$)	8.5 1.5 0.38	71.0 4.5 0.40	39.9 4.4 0.01
4	Intermediate waters	Depth $= 500$–1000 m $[O_2] = 5$–$70\,\mu mol\,L^{-1}$ $[NO_2^-] < 0.02\,\mu mol\,L^{-1}$	Produced N_2O Standard error R^2 ($n = 21$)	3.6 0.6 0.69	50.0 2.4 0	15.6 4.1 0.04
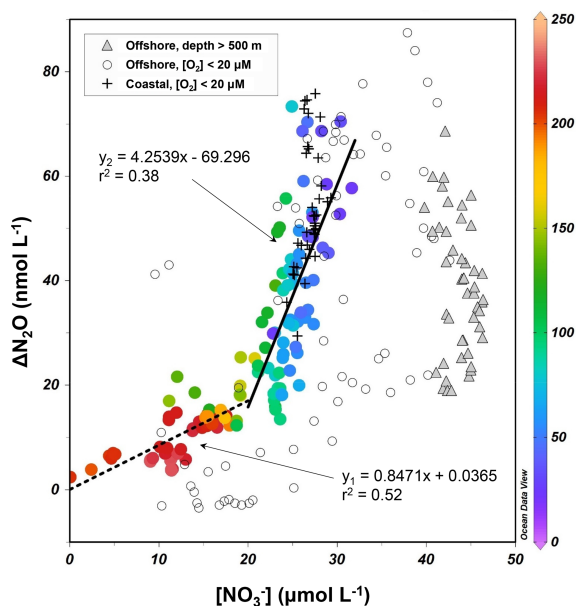
Figure 6. NO_3^-–ΔN_2O relationship for samples from the upper oxycline ($[O_2] > 20\,\mu mol\,L^{-1}$, depth < 500 m, colored circles), low-oxygen ($[O_2] < 20\,\mu mol\,L^{-1}$) coastal waters (+), low-oxygen offshore waters (open circles), and the lower oxycline (depth > 500 m, filled triangles). Color bar shows the O_2 concentrations ($\mu mol\,L^{-1}$). For samples with NO_3^- concentrations higher and lower than $20\,\mu mol\,L^{-1}$, two linear regressions were performed separately.

produced) of $0.17 \pm 0.02\,\%$. At $[NO_3^-] > 20\,\mu mol\,L^{-1}$ (corresponding to $[O_2] < 100\,\mu mol\,L^{-1}$) the yield increases to $0.85 \pm 0.13\,\%$.

These N_2O yield estimates are generally comparable to previously reported values ($0.04\,\%$–$1.6\,\%$) in the ETSP

(Elkins et al., 1978; Ji et al., 2015), and indicate that potential N_2O production from NH_4^+ oxidation decreases with water column oxygenation due to intrusion of oxygen-rich water masses (Llanillo et al., 2013; Graco et al., 2017), as well as El Niño-induced oxygenation (see Sect. 4.3). As discussed earlier, the oxycline samples were probably influenced by mixing of suboxic water with active denitrification, producing high N_2O concentrations and low NO_3^- concentrations; the N_2O yield estimates here are thus spatially and temporally integrated. As a comparison, the ^{15}N tracer incubation method directly measured $0.04\,\%$ N_2O yield during NH_4^+ oxidation at $[O_2] > 100\,\mu mol\,L^{-1}$ (Ji et al., 2015).

4.3 N_2O distribution and fluxes during El Niño

Excess N_2O (ΔN_2O) in surface waters is one of the principal factors regulating sea-to-air N_2O fluxes. To evaluate the effect of strong El Niño on oceanic N_2O fluxes, we compare surface and water column ΔN_2O concentrations in shelf waters (< 300 m depth) along 8–16° S during El Niño (October 2015) and neutral conditions (December 2012). In the ETSP, higher surface ΔN_2O concentrations and thus higher potential N_2O efflux occurred at nearshore waters. Generally, the surface ΔN_2O concentrations in October 2015 (Fig. 7a) were lower than those of December 2012 (Fig. 7d); the highest surface ΔN_2O concentrations were 50 and $250\,nmol\,L^{-1}$ in 2015 and 2012, respectively. The region of high surface ΔN_2O occurred near ~ 14 and $\sim 10°$ S in 2015 and in 2012, respectively. It appears that N_2O efflux was significantly reduced during El Niño; in October 2015, coastal water had a N_2O flux of 23–$108\,\mu mol\,m^{-2}\,d^{-1}$ (Fig. 5c), much lower than that of December 2012 having 459–$1825\,\mu mol\,m^{-2}\,d^{-1}$ (Arévalo-Martínez et al., 2015). Such a $75\,\%$–$95\,\%$ reduction in N_2O fluxes dur-
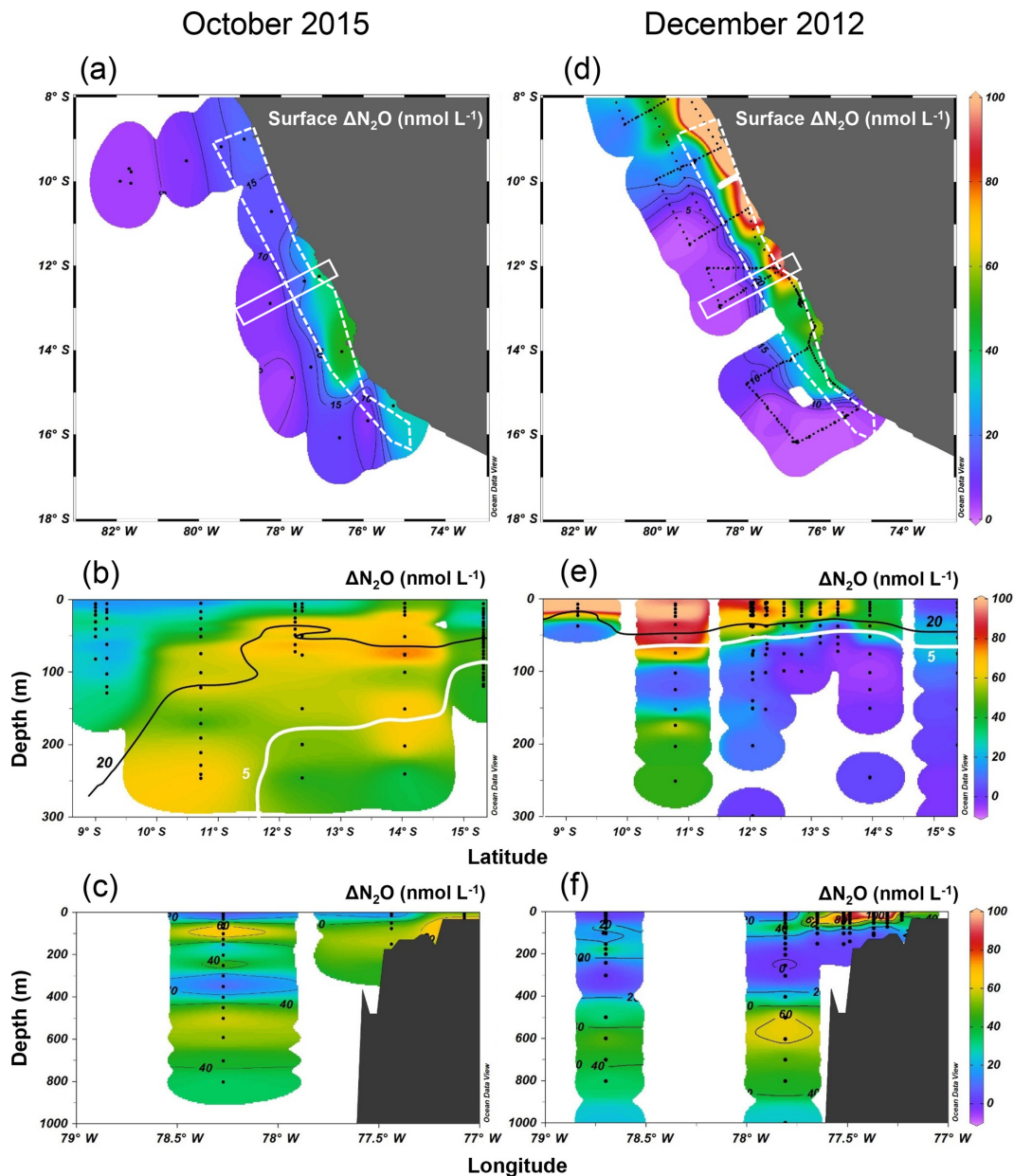
October 2015   December 2012

Figure 7. Surface ΔN_2O **(a, d)**, meridional water column ΔN_2O distribution **(b, e)**, and zonal water column ΔN_2O distribution **(c, f)** in October 2015 and in December 2012. Color bars for ΔN_2O (nmol L^{-1}) are shown in **(d)**, **(e)**, and **(f)**. For meridional ΔN_2O distribution **(b, e)**, data are from the coastal section, shown as a white dashed polygon in panels **(a)** and **(d)**. For zonal ΔN_2O distribution **(c, f)**, data are from a section 12–13° S, shown as a white rectangle. In **(b)** and **(e)** the "20" contour line (black) denotes the $[O_2] = 20\,\mu mol\,L^{-1}$ isoline, equivalent to the lower boundary of the oxygenated layer; the "5" contour line (white) denotes the $[O_2] = 5\,\mu mol\,L^{-1}$ isoline, equivalent to the upper boundary of the oxygen-deficient zone.

ing the 2015–2016 El Niño in the ETSP was comparable to an 80 % reduction in fluxes observed in the central equatorial Pacific during the 1982–1983 El Niño (Cline et al., 1987).

Suppressed upwelling or increased downwelling during El Niño events, as observed in both observational and model studies (Llanillo et al., 2013; Graco et al., 2017; Mogollón and Calil, 2017), can directly and indirectly affect N$_2$O fluxes to the atmosphere: first, reduced upward transport of sub-

surface N$_2$O-rich water not only decreased surface ΔN_2O, but also increased subsurface ΔN_2O, which is illustrated by the comparative observation of higher subsurface ΔN_2O concentrations in coastal waters in October 2015 (Fig. 7b, c) than those in December 2012 (Fig. 7e, f). Second, because the oxygen sensitivity of the denitrification sequence increases with each step (Körner and Zumft, 1989), El Niño-induced water column oxygenation inhibited N$_2$O consump-
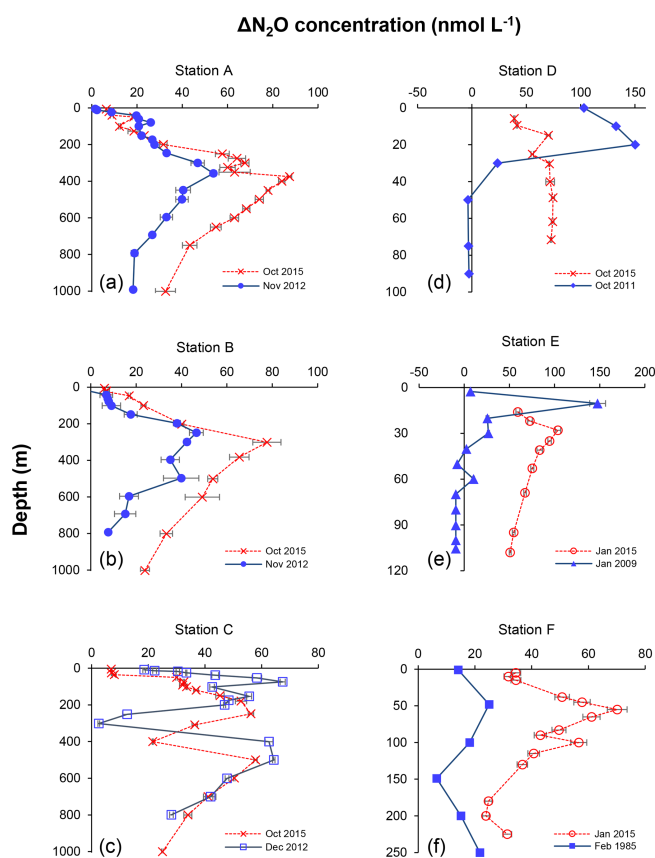
Figure 8. Depth profiles of N_2O concentration excess (ΔN_2O, $nmol\,L^{-1}$) measured at six different stations representing offshore **(a, b, c)** and coastal waters **(d, e, f)** during February 1985 (filled squares in **f**), January 2009 (filled triangles in **e**), October 2011 (filled diamonds in **d**), November 2012 (filled circles in **a** and **b**), December 2012 (open squares in **c**), January 2015 (open circles in **e** and **f**), and October 2015 (crosses). Profiles of 2015 are indicated in red and other years in blue. Error bars represent standard deviation of repeated measurements.
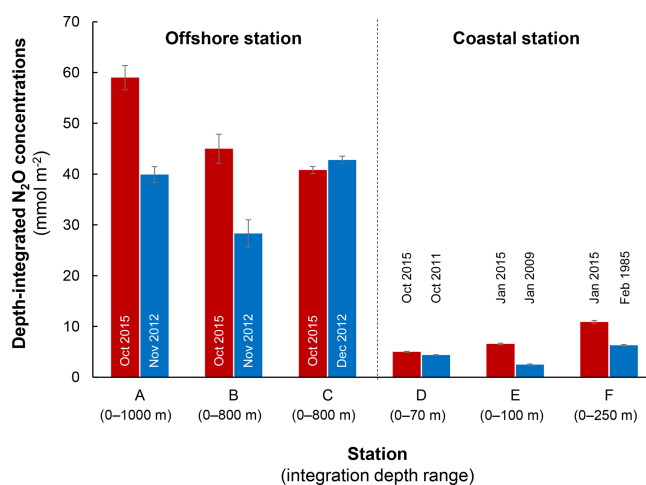

Figure 9. Comparison of depth-integrated N_2O concentrations between El Niño (red bars) and normal years (blue bars). Stations A, B, and C are characterized as offshore stations whereas D, E, and F are coastal stations. Error bars represent propagation of error from analytical precision of respective N_2O concentration profiles. See Fig. 2a for station locations and Table S1 for data sources.

tion within the ODZ (bounded by $[O_2] = 5\,\mu mol\,L^{-1}$ isoline), as demonstrated by the disappearance of N_2O undersaturation ($\Delta N_2O < 0$) in coastal water in 2015 (Fig. 7b, c), contrasting water column N_2O undersaturation occurring at 100 m at 13–14° S in December 2012 (Fig. 7e, f). Third, as shown in this study, the deepening and expansion of the suboxic zone ($[O_2] = 5$–$20\,\mu mol\,L^{-1}$) caused by the El Niño event stimulated subsurface N_2O production via denitrification, as demonstrated by the close spatial coupling between local maximum ΔN_2O concentrations and the oxycline ($[O_2] = 5$ and $20\,\mu mol\,L^{-1}$ isolines, Fig. 7b and e). Lastly, upwelling of oxygen-rich water along the Peruvian coast, especially north of 12° S (Stramma et al., 2016), inhibited local N_2O production and caused the southward relocation of surface ΔN_2O "hot spots".

The decrease in surface ΔN_2O concentration during El Niño was associated with an increase in subsurface N_2O con-

centrations. Water column ΔN_2O concentration profiles at expanded temporal and spatial coverage (see Fig. 2a for location map and Table S1 for coordinates) were compared within the same season between El Niño and non-El Niño years (Fig. 8). We included N_2O data from January 2015 when the highest ONI was recorded during austral summer (Fig. 1). These comparisons at offshore stations were made to cover the depth ranges with pronounced El Niño effects and available data (1000 m at station A and 800 m at stations B and C). At coastal stations the depth ranges were station bottom depth (stations D and E) or 250 m (station F). Generally, subsurface ΔN_2O concentration peaks were observed at deeper depths during 2015. Offshore stations had higher subsurface peak ΔN_2O concentrations during El Niño (Fig. 8a, b), except at station C where the peak concentration during October 2015 was comparable to that of December 2012 (Fig. 8c). At coastal stations D and E, higher ΔN_2O concentrations were found below 50 m but peak ΔN_2O concentrations were lower during El Niño years (Fig. 8d, e). At the southernmost coastal station F, the peak ΔN_2O concentration was higher in 2015 than that of 1985; both were found at similar depths at ~ 60 m. The increase in subsurface N_2O concentrations during El Niño resulted in the OMZ water column retaining a larger amount of N_2O, as shown by higher depth-integrated N_2O concentrations during El Niño years than non-El Niño years in both coastal and offshore waters (Fig. 9).

In all, the apparent decrease in N_2O efflux during strong El Niño events in the tropical Pacific, as shown in this study and others (Cline et al., 1987; Butler et al., 1989) is the result of complex physical and biochemical changes. The above

comparative analyses are simple due to limited data availability. Consequently, these following aspects are yet to be resolved: (1) it is unclear how offshore N_2O fluxes vary from neutral to El Niño years. Current ΔN_2O profiles show higher surface ΔN_2O concentrations at stations A and B in 2015 (Fig. 8a and b), whereas the surface ΔN_2O was lower in 2015 at station C (Fig. 8c). A zonal (east–west) section near $12°$ S showed slightly higher offshore surface ΔN_2O in 2015 ($\sim 5\ \mathrm{nmol\,L^{-1}}$, Fig. 7c) than in 2012 ($\sim 1\ \mathrm{nmol\,L^{-1}}$, Fig. 7f). The decrease in coastal N_2O fluxes during El Niño could be compensated for by increase in offshore fluxes. (2) The southward relocation of high surface ΔN_2O from neutral to El Niño years (Fig. 7a and d) possibly results in higher surface ΔN_2O and hence higher N_2O flux in the southern region of the ETSP (e.g., south of $16°$ S; Fig. 8f). (3) Complex hydrographical changes during the El Niño event resulted in the deepening of the ODZ boundary and the depths of peak N_2O concentration. It is possible that these chemical features occur in similar potential density surfaces (with respect to non-El Niño conditions) that are deepened during El Niño, or they occur in different potential density surfaces during El Niño, or a combination of both. (4) It is possible that once the normal upwelling is resumed after the El Niño event, N_2O produced and retained in the subsurface layer in coastal and offshore waters could be a potential reservoir contributing to high N_2O fluxes. (5) The co-occurrence of El Niño and mesoscale eddy formation along the Peruvian coast will have complicated effects on N_2O fluxes, which remains unexplored.

5   Conclusions

The eastern tropical South Pacific is a major oceanic upwelling region with N_2O effluxes and active water column production affected by strong El Niño events. During a developing strong El Niño event in October 2015, a more pronounced warming effect occurred at lower latitudes in the ETSP. In comparison to conditions in December 2012 (non-El Niño), deepening of the oxygen-deficient zone's upper boundary occurred at coastal waters in October 2015, coinciding with lower peak N_2O concentrations at deeper depths. Shelf N_2O effluxes were significantly lower during the 2015 El Niño as a result of lower surface levels of N_2O supersaturation. However, a change in upwelling pattern appeared to cause higher subsurface N_2O concentrations and increased the water column N_2O inventories during El Niño than in other non-El Niño years. Natural abundance isotopic and isotopomeric analysis indicated that both nitrification and denitrification are important pathways for N_2O production, and denitrification-derived N_2O near the suboxic waters probably contributes to the efflux to the atmosphere. Decreased N_2O efflux and subsurface accumulation during strong El Niño events are likely the result of suppressed upwelling and a decrease in water column oxygen consumption. The current

dataset represents a "snapshot" of a developing El Niño event that lasted 18 months; thus the complex spatial and temporal patterns of El Niño-induced N_2O distribution in ETSP remain to be explored.

References

Anderson, J. H.: The metabolism of hydroxylamine to nitrite by Nitrosomonas, Biochem. J., 91, 8–17, 1964.

Arévalo-Martínez, D. L., Kock, A., Loscher, C. R., Schmitz, R. A., and Bange, H. W.: Massive nitrous oxide emissions from the tropical South Pacific Ocean, Nat. Geosci., 8, 530–533, https://doi.org/10.1038/ngeo2469, 2015.

Arévalo-Martínez, D. L., Kock, A., Löscher, C. R., Schmitz, R. A., Stramma, L., and Bange, H. W.: Influence of mesoscale eddies on the distribution of nitrous oxide in the eastern tropical South Pacific, Biogeosciences, 13, 1105–1118, https://doi.org/10.5194/bg-13-1105-2016, 2016.

Babbin, A. R., Bianchi, D., Jayakumar, A., and Ward, B. B.: Rapid nitrous oxide cycling in the suboxic ocean, Science, 348, 1127–1129, https://doi.org/10.1126/science.aaa8380, 2015.

Barber, R. T. and Chavez, F. P.: Biological Consequences of El Niño, Science, 222, 1203–1210, https://doi.org/10.1126/science.222.4629.1203, 1983.

Blasing, T.: Recent greenhouse gas concentrations, Carbon Dioxide Information Analysis Center (CDIAC), Oak Ridge National Laboratory (ORNL), Oak Ridge, TN, USA, 2016.

Bonin, P., Gilewicz, M., and Bertrand, J. C.: Effects of oxygen on each step of denitrification on Pseudomonas nautica, Can. J. Microbiol., 35, 1061–1064, https://doi.org/10.1139/m89-177, 1989.

Bourbonnais, A., Letscher, R. T., Bange, H. W., Échevin, V., Larkum, J., Mohn, J., Yoshida, N., and Altabet, M. A.: N$_2$O production and consumption from stable isotopic and concentration data in the Peruvian coastal upwelling system, Global Biogeochem. Cy., 31, 678–698, https://doi.org/10.1002/2016GB005567, 2017.

Butler, J. H., Elkins, J. W., Thompson, T. M., and Egan, K. B.: Tropospheric and dissolved N$_2$O of the west Pacific and east Indian Oceans during the El Niño Southern Oscillation event of 1987, J Geophys. Res.-Atmos., 94, 14865–14877, https://doi.org/10.1029/JD094iD12p14865, 1989.

Carrasco, C., Karstensen, J., and Farias, L.: On the Nitrous Oxide Accumulation in Intermediate Waters of the Eastern South Pacific Ocean, Front. Mar. Sci., 4, 24, https://doi.org/10.3389/fmars.2017.00024, 2017.

Chavez, F. P., Ryan, J., Lluch-Cota, S. E., and Ñiquen C. M.: From Anchovies to Sardines and Back: Multidecadal Change in the Pacific Ocean, Science, 299, 217–221, https://doi.org/10.1126/science.1075880, 2003.

Cline, J. D., Wisegarver, D. P., and Kelly-Hansen, K.: Nitrous oxide and vertical mixing in the equatorial Pacific during the 1982–1983 El Niño, Deep-Sea. Res., 34, 857–873, https://doi.org/10.1016/0198-0149(87)90041-0, 1987.

Codispoti, L. A. and Christensen, J. P.: Nitrification, denitrification and nitrous oxide cycling in the eastern tropical South Pacific ocean, Mar. Chem., 16, 277–300, https://doi.org/10.1016/0304-4203(85)90051-9, 1985.

Cornejo, M., Murillo, A. A., and Farías, L.: An unaccounted for N$_2$O sink in the surface water of the eastern subtropical South

Pacific: Physical versus biological mechanisms, Prog. Oceanogr., 137, 12–23, https://doi.org/10.1016/j.pocean.2014.12.016, 2015.

Elkins, J. W., Wofsy, S. C., Mcelroy, M. B., Kolb, C. E., and Kaplan, W. A.: Aquatic sources and sinks for nitrous oxide, Nature, 275, 602–606, https://doi.org/10.1038/275602a0, 1978.

Espinoza-Morriberón, D., Echevin, V., Colas, F., Tam, J., Ledesma, J., Vásquez, L., and Graco, M.: Impacts of El Niño events on the Peruvian upwelling system productivity, J. Geophys. Res.-Oceans, 122, 5423–5444, https://doi.org/10.1002/2016JC012439, 2017.

Farías, L., Castro-González, M., Cornejo, M., Charpentier, J., Faúndez, J., Boontanon, N., and Yoshida, N.: Denitrification and nitrous oxide cycling within the upper oxycline of the eastern tropical South Pacific oxygen minimum zone, Limnol. Oceanogr., 54, 132–144, https://doi.org/10.4319/lo.2009.54.1.0132, 2009.

Farías, L., Faúndez, J., Fernández, C., Cornejo, M., Sanhueza, S., and Carrasco, C.: Biological N$_2$O Fixation in the Eastern South Pacific Ocean and Marine Cyanobacterial Cultures, PLOS ONE, 8, e63956, https://doi.org/10.1371/journal.pone.0063956, 2013.

Frame, C. H. and Casciotti, K. L.: Biogeochemical controls and isotopic signatures of nitrous oxide production by a marine ammonia-oxidizing bacterium, Biogeosciences, 7, 2695–2709, https://doi.org/10.5194/bg-7-2695-2010, 2010.

Fujii, A., Toyoda, S., Yoshida, O., Watanabe, S., Sasaki, K. I., and Yoshida, N.: Distribution of nitrous oxide dissolved in water masses in the eastern subtropical North Pacific and its origin inferred from isotopomer analysis, J. Oceanogr., 69, 147–157, https://doi.org/10.1007/s10872-012-0162-4, 2013.

Garcia, H. E. and Gordon, L. I.: Oxygen solubility in seawater: Better fitting equations, Limnol. Oceanogr., 6, 1307–1312, https://doi.org/10.4319/lo.1992.37.6.1307, 1992.

Graco, M. I., Purca, S., Dewitte, B., Castro, C. G., Morón, O., Ledesma, J., Flores, G., and Gutiérrez, D.: The OMZ and nutrient features as a signature of interannual and low-frequency variability in the Peruvian upwelling system, Biogeosciences, 14, 4601–4617, https://doi.org/10.5194/bg-14-4601-2017, 2017.

Grundle, D. S., Maranger, R., and Juniper, S. K.: Upper Water Column Nitrous Oxide Distributions in the Northeast Subarctic Pacific Ocean, Atmos. Ocean, 50, 475–486, https://doi.org/10.1080/07055900.2012.727779, 2012.

Grundle, D. S., Löscher, C. R., Krahmann, G., Altabet, M. A., Bange, H. W., Karstensen, J., Körtzinger, A., and Fiedler, B.: Low oxygen eddies in the eastern tropical North Atlantic: Implications for N$_2$O cycling, Sci. Rep.-UK, 7, 4806, https://doi.org/10.1038/s41598-017-04745-y, 2017.

Haskell, W. Z., Kadko, D., Hammond, D. E., Knapp, A. N., Prokopenko, M. G., Berelson, W. M., and Capone, D. G.: Upwelling velocity and eddy diffusivity from [7]Be measurements used to compare vertical nutrient flux to export POC flux in the Eastern Tropical South Pacific, Mar. Chem., 168, 140–150, https://doi.org/10.1016/j.marchem.2014.10.004, 2015.

Ji, Q., Babbin, A. R., Jayakumar, A., Oleynik, S., and Ward, B. B.: Nitrous oxide production by nitrification and denitrification in the Eastern Tropical South Pacific oxygen minimum zone, Geophys. Res. Lett., 42, 10755–10764, https://doi.org/10.1002/2015GL066853, 2015.

Kock, A. and Bange, H. W.: Counting the ocean's greenhouse gas emissions, Eos, 96, https://doi.org/10.1029/2015EO023665, 2015.

Kock, A., Arévalo-Martínez, D. L., Löscher, C. R., and Bange, H. W.: Extreme N$_2$O accumulation in the coastal oxygen minimum zone off Peru, Biogeosciences, 13, 827–840, https://doi.org/10.5194/bg-13-827-2016, 2016.

Körner, H. and Zumft, W. G.: Expression of denitrification enzymes in response to the dissolved oxygen level and respiratory substrate in continuous culture of Pseudomonas stutzeri, Appl. Environ. Microbiol., 55, 1670–1676, 1989.

Llanillo, P. J., Karstensen, J., Pelegrí, J. L., and Stramma, L.: Physical and biogeochemical forcing of oxygen and nitrate changes during El Niño/El Viejo and La Niña/La Vieja upper-ocean phases in the tropical eastern South Pacific along 86° W, Biogeosciences, 10, 6339–6355, https://doi.org/10.5194/bg-10-6339-2013, 2013.

Mogollón, R. and Calil, P. H. R.: On the effects of ENSO on ocean biogeochemistry in the Northern Humboldt Current System (NHCS): A modeling study, J. Marine Syst., 172, 137–159, https://doi.org/10.1016/j.jmarsys.2017.03.011, 2017.

Mohn, J., Wolf, B., Toyoda, S., Lin, C.-T., Liang, M.-C., Brüggemann, N., Wissel, H., Steiker Amy, E., Dyckmans, J., Szwec, L., Ostrom Nathaniel, E., Casciotti Karen, L., Forbes, M., Giesemann, A., Well, R., Doucett Richard, R., Yarnes Chris, T., Ridley Anna, R., Kaiser, J., and Yoshida, N.: Interlaboratory assessment of nitrous oxide isotopomer analysis by isotope ratio mass spectrometry and laser spectroscopy: current status and perspectives, Rapid Commun. Mass Sp., 28, 1995–2007, https://doi.org/10.1002/rcm.6982, 2014.

Mothet, A., Sebilo, M., Laverman, A. M., Vaury, V., and Mariotti, A.: Is site preference of N$_2$O a tool to identify benthic denitrifier N$_2$O?, Environ. Chem., 10, 281–284, https://doi.org/10.1071/EN13021, 2013.

Ñiquen, M. and Bouchon, M.: Impact of El Niño events on pelagic fisheries in Peruvian waters, Deep-Sea Res. Pt., 2, 51, 563–574, https://doi.org/10.1016/j.dsr2.2004.03.001, 2004.

Peng, X., Fuchsman, C. A., Jayakumar, A., Warner, M. J., Devol, A. H., and Ward, B. B.: Revisiting nitrification in the Eastern Tropical South Pacific: A focus on controls, J. Geophys. Res.-Oceans, 121, 1667–1684, https://doi.org/10.1002/2015JC011455, 2016.

Philander, S. G. H.: El Nino Southern Oscillation phenomena, Nature, 302, 295–301, https://doi.org/10.1038/302295a0, 1983.

Popp, B. N., Westley, M. B., Toyoda, S., Miwa, T., Dore, J. E., Yoshida, N., Rust, T. M., Sansone, F. J., Russ, M. E., Ostrom, N. E., and Ostrom, P. H.: Nitrogen and oxygen isotopomeric constraints on the origins and sea-to-air flux of N$_2$O in the oligotrophic subtropical North Pacific gyre, Global Biogeochem. Cy., 16, 12-11–12-10, https://doi.org/10.1029/2001GB001806, 2002.

Ravishankara, A., Daniel, J. S., and Portmann, R. W.: Nitrous oxide (N$_2$O): the dominant ozone-depleting substance emitted in the 21st century, Science, 326, 123–125, https://doi.org/10.1126/science.1176985, 2009.

Rees, A. P., Brown, I. J., Clark, D. R., and Torres, R.: The Lagrangian progression of nitrous oxide within filaments formed in the Mauritanian upwelling, Geophys. Res. Lett., 38, L21606, https://doi.org/10.1029/2011GL049322, 2011.

Revsbech, N. P., Larsen, L. H., Gundersen, J., Dalsgaard, T., Ulloa, O., and Thamdrup, B.: Determination of ultralow oxygen concentrations in oxygen minimum zones by

the STOX sensor, Limnol. Oceanogr.-Meth., 7, 371–381, https://doi.org/10.4319/lom.2009.7.371, 2009.

Santoso, A., Mcphaden, M. J., and Cai, W.: The defining characteristics of ENSO extremes and the strong 2015/2016 El Niño, Rev. Geophys., 55, 1079–1129, https://doi.org/10.1002/2017RG000560, 2017.

Silva, N., Rojas, N., and Fedele, A.: Water masses in the Humboldt Current System: Properties, distribution, and the nitrate deficit as a chemical water mass tracer for Equatorial Subsurface Water off Chile, Deep-Sea Res. Pt. 2, 56, 1004–1020, https://doi.org/10.1016/j.dsr2.2008.12.013, 2009.

Stramma, L., Fischer, T., Grundle, D. S., Krahmann, G., Bange, H. W., and Marandino, C. A.: Observed El Niño conditions in the eastern tropical Pacific in October 2015, Ocean Sci., 12, 861–873, https://doi.org/10.5194/os-12-861-2016, 2016.

Strub, P. T., Mesías, J. M., Montecino, V., Rutillant, J., and Salinas, S.: Coastal ocean circulation off western south America,, in: The Sea, edited by: Robinson, A. R. and Brink, K. H., John Wiley, New York, 273–313, 1998.

Toyoda, S., Yano, M., Nishimura, S.-i., Akiyama, H., Hayakawa, A., Koba, K., Sudo, S., Yagi, K., Makabe, A., Tobari, Y., Ogawa, N. O., Ohkouchi, N., Yamada, K., and Yoshida, N.: Characterization and production and consumption processes of N$_2$O emitted from temperate agricultural soils determined via isotopomer ratio analysis, Global Biogeochem. Cy., 25, GB2008, https://doi.org/10.1029/2009GB003769, 2011.

Toyoda, S., Yoshida, N., and Koba, K.: Isotopocule analysis of biologically produced nitrous oxide in various environments, Mass Spectrom. Rev., 36, 135–160, https://doi.org/10.1002/mas.21459, 2017.

Trimmer, M., Chronopoulou, P.-M., Maanoja, S. T., Upstill-Goddard, R. C., Kitidis, V., and Purdy, K. J.: Nitrous oxide as a function of oxygen and archaeal gene abundance in the North Pacific, Nat. Commun., 7, 13451, https://doi.org/10.1038/ncomms13451, 2016.

Walter, S., Breitenbach, U., Bange, H. W., Nausch, G., and Wallace, D. W. R.: Distribution of N$_2$O in the Baltic Sea during transition from anoxic to oxic conditions, Biogeosciences, 3, 557–570, https://doi.org/10.5194/bg-3-557-2006, 2006.

Wanninkhof, R.: Relationship between wind speed and gas exchange over the ocean revisited, Limnol. Oceanogr.-Meth., 12, 351–362, https://doi.org/10.4319/lom.2014.12.351, 2014.

Weiss, R. F. and Price, B. A.: Nitrous oxide solubility in water and seawater, Mar. Chem., 8, 347–359, https://doi.org/10.1016/0304-4203(80)90024-9, 1980.

Well, R., Flessa, H., Jaradat, F., Toyoda, S., and Yoshida, N.: Measurement of isotopomer signatures of N$_2$O in groundwater, J. Geophys. Res.-Biogeo., 110, G02006, https://doi.org/10.1029/2005JG000044, 2005.

Winther, M., Balslev-Harder, D., Christensen, S., Priemé, A., Elberling, B., Crosson, E., and Blunier, T.: Continuous measurements of nitrous oxide isotopomers during incubation experiments, Biogeosciences, 15, 767–780, https://doi.org/10.5194/bg-15-767-2018, 2018.

Yamagishi, H., Westley, M. B., Popp, B. N., Toyoda, S., Yoshida, N., Watanabe, S., Koba, K., and Yamanaka, Y.: Role of nitrification and denitrification on the nitrous oxide cycle in the eastern tropical North Pacific and Gulf of California, J Geophys. Res.-

Biogeo., 112, G02015, https://doi.org/10.1029/2006JG000227, 2007.

Yang, S., Gruber, N., Long, M. C., and Vogt, M.: ENSO-Driven Variability of Denitrification and Suboxia in the Eastern Tropical Pacific Ocean, Global Biogeochem. Cy., 31, 1470–1487, https://doi.org/10.1002/2016GB005596, 2017.

Yoshida, N. and Toyoda, S.: Constraining the atmospheric N_2O budget from intramolecular site preference in N_2O isotopomers, Nature, 405, 330–334, https://doi.org/10.1038/35012558, 2000.